Models for integrated and differential scattering optical properties of encapsulated light absorbing carbon aggregates

Michael Kahnert,[1,2,*] **Timo Nousiainen,**[3] **and Hannakaisa Lindqvist,**[3]

[1]*Swedish Meteorological and Hydrological Institute (SMHI), Research Department, Folkborgsvägen 17, SE-601 76 Norrköping, Sweden*
[2] *Chalmers University of Technology, Department of Earth and Space Science, SE-412 96 Gothenburg, Sweden*
[3] *Department of Physics, P. O. Box 48, FI-00014 University of Helsinki, Finland*

[*] *michael.kahnert@smhi.se*

Abstract: Optical properties of light absorbing carbon (LAC) aggregates encapsulated in a shell of sulfate are computed for realistic model geometries based on field measurements. Computations are performed for wavelengths from the UV-C to the mid-IR. Both climate- and remote sensing-relevant optical properties are considered. The results are compared to commonly used simplified model geometries, none of which gives a realistic representation of the distribution of the LAC mass within the host material and, as a consequence, fail to predict the optical properties accurately. A new core-gray shell model is introduced, which accurately reproduces the size- and wavelength dependence of the integrated and differential optical properties.

OCIS codes: (290.5850) Scattering, particles; (010.1110) Aerosols; (010.1310) Atmospheric scattering; (290.5825) Scattering theory; (290.1350) Backscattering; (010.1290) Atmospheric optics; (010.0280) Remote sensing and sensors.

References and links

1. A. R. Jones, "Light scattering in combustion," in *Light Scattering Reviews,* A. Kokhanovsky, ed. (Springer, 2006).
2. M. Schnaiter, H. Horvath, O. Möhler, K.-H. Naumann, H. Saathoff, and O. W. Schöck, "UV-VIS-NIR spectral optical properties of soot and soot-containing aerosols," J. Aerosol Sci. **34**, 1421–1444 (2003).
3. J. Hallett, J. G. Hudson, and C. F. Rogers, "Characterization of combustion aerosols for haze and cloud formation," Aerosol Sci. Technol. **10**, 70–83 (1989).
4. I. Colbeck, L. Appleby, E. J. Hardman, and R. M. Harrison, "The optical properties and morphology of cloud-processed carbonaceous smoke," J. Aerosol Sci. **21**, 527–538 (1990).
5. G. Ramachandran and P. C. Reist, "Characterization of morphological changes in agglomerates subject to condensation and evaporation using multiple fractal dimensions," Aerosol Sci. Technol. **23**, 431–442 (1995).
6. S. Nyeki and I. Colbeck, "Fractal dimension analysis of single, in-situ, restructured carbonaceous aggregates," Aerosol Sci. Technol. **23**, 109–120 (1995).
7. N. Riemer, H. Vogel, and B. Vogel, "Soot aging time scales in polluted regions during day and night," Atmos. Chem. Phys. **4**, 1885–1893 (2004).
8. S. Tsyro, D. Simpson, L. Tarrasón, Z. K. K. Kupiainen, C. Pio, and K. E. Yttri, "Modelling of elemental carbon over Europe," J. Geophys. Res. **112**, D23S19, doi:10.1029/2006JD008164 (2007).
9. B. Croft, U. Lohmann, and K. von Salzen, "Black carbon aging in the Canadian Centre for Climate modelling and analysis atmospheric general circulation model," Atmos. Chem. Phys. **5**, 1383–1419 (2005).

10. R. J. Park, D. J. Jacob, P. I. Palmer, A. D. Clarke, R. J. Weber, M. A. Zondlo, F. L. Eisele, A. R. Bandy, D. C. Thornton, G. W. Sachse, and T. C. Bond, "Export efficiency of black carbon aerosol in continental outflow: Global implications," J. Geophys. Res. **110**, D11205, doi:10.1029/2004JD005432 (2005).

11. A. Worringen, M. Ebert, T. Trautmann, S. Weinbruch, and G. Helas, "Optical properties of internally mixed ammonium sulfate and soot particles–a study of individual aerosol particles and ambient aerosol populations," Appl. Opt. **47**, 3835–3845 (2008).

12. B. Scarnato, S. Vahidinia, D. T. Richard, and T. W. Kirchstetter, "Effects of internal mixing and aggregate morphology on optical properties of black carbon using a discrete dipole approximation model," Atmos. Chem. Phys. Discuss. **12**, 26401–26434 (2012).

13. K. Adachi and P. R. Buseck, "Internally mixed soot, sulfates, and organic matter in aerosol particles from Mexico City," Atmos. Chem. Phys. **8**, 6469–6481 (2008).

14. T. C. Bond, G. Habib, and R. W. Bergstrom, "Limitations in the enhancement of visible light absorption due to mixing state," J. Geophys. Res. **111**, D20211, doi:10.1029/2006JD007315 (2006).

15. M. Kahnert, T. Nousiainen, H. Lindqvist, and M. Ebert, "Optical properties of light absorbing carbon aggregates mixed with sulfate: assessment of different model geometries for climate forcing calculations," Opt. Express **20**, 10042–10058 (2012).

16. M. Kahnert, "On the discrepancy between modelled and measured mass absorption cross sections of light absorbing carbon aerosols," Aerosol Sci. Technol. **44**, 453–460 (2010).

17. M. I. Mishchenko, V. P. Tishkovets, L. D. Travis, B. Cairns, J. M. Dlugach, L. Liu, V. K. Rosenbush, and N. N. Kiselev, "Electromagnetic scattering by a morphologically complex object: Fundamental concepts and common misconceptions," J. Quant. Spectrosc. Radiat. Transfer **112**, 671–692 (2011).

18. M. Kahnert, "Modelling the optical and radiative properties of freshly emitted light absorbing carbon within an atmospheric chemical transport model," Atmos. Chem. Phys. **10**, 1403–1416 (2010).

19. M. Kahnert, "Numerically exact computation of the optical properties of light absorbing carbon aggregates for wavelength of 200 nm V 12.2 μm," Atmos. Chem. Phys. **10**, 8319–8329 (2010).

20. M. Kahnert and A. Devasthale, "Black carbon fractal morphology and short-wave radiative impact: a modelling study," Atmos. Chem. Phys. **11**, 11745–11759 (2011).

21. P. Chýlek, G. Videen, D. J. W. Geldart, J. S. Dobbie, and H. C. W. Tso, "Effective medium approximations for heterogeneous particles," in *Light Scattering by Nonspherical Particles,* , M. I. Mishchenko, J. W. Hovenier, and L. D. Travis, eds. (Academic, 2000), pp. 274–308.

22. G. Videen and P. Chýlek, "Scattering by a composite sphere with an absorbing inclusion and effective medium approximations," Opt. Commun. **158**, 1–6 (1998).

23. M. Z. Jacobson, "Strong radiative heating due to the mixing state of black carbon in atmospheric aerosols," Nature **409**, 695–697 (2001).

24. K. Adachi, S. Chung, and P. R. Buseck, "Shapes of soot aerosol particles and implications for their effects on climate," J. Geophys. Res. **115**, D15206, doi:10.1029/2009JD012868 (2010).

25. M. Wentzel, G. Gorzawski, K.-H. Naumann, H. Saathoff, and S. Weinbruch, "Transmission electron microscopical and aerosol dynamical characterization of soot aerosols," Aerosol Sci. **34**, 1347–1370 (2003).

26. J. C. Maxwell Garnett, "Colours in metal glasses and in metallic films," Philos. Trans. R. Soc. A **203**, 385–420 (1904).

27. M. Kahnert, "Irreducible representations of finite groups in the T matrix formulation of the electromagnetic scattering problem," J. Opt. Soc. Am. A **22**, 1187–1199 (2005).

28. H. Chang and T. T. Charalampopoulos, "Determination of the wavelength dependence of refractive indices of flame soot," Proc. R. Soc. Lond. A **430**, 577–591 (1990).

29. T. C. Bond and R. W. Bergstrom, "Light absorption by carbonaceous particles: An investigative review," Aerosol Sci. Technol. **40**, 27–67 (2006).

30. M. Hess, P. Koepke, and I. Schult, "Optical properties of aerosols and clouds: The software package OPAC," Bull. Am. Met. Soc. **79**, 831–844 (1998).

31. B. T. Draine and P. J. Flatau, "Discrete-dipole approximation for scattering calculations," J. Opt. Soc. Am. A **11**, 1491–1499 (1994).

32. B. T. Draine and J. J. Goodman, "Beyond Clausius-Mossotti: Wave propagation on a polarizable point lattice and the discrete dipole approximation," Astrophysical J. **405**, 685–697 (1993).

33. D. W. Mackowski and M. I. Mishchenko, "Calculation of the T matrix and the scattering matrix for ensembles of spheres," J. Opt. Soc. Am. A **13**, 2266–2278 (1996).

34. K. Schmidt, M. Yurkin, and M. Kahnert, "A case study on the reciprocity in light scattering computations," Opt. Express **20**, 23253–23274 (2012).

35. D. Gutkowicz-Krusin and B. T. Draine, "Propagation of electromagnetic waves on a rectangular lattice of polarizable points," Tech. rep., http://arxiv.org/abs/astro-ph/0403082 (2004).

36. M. I. Mishchenko, , L. D. Travis, and A. A. Lacis, *Scattering, Absorption, and Emission of Light by Small Particles* (Cambridge University, 2002).

37. O. B. Toon and T. P. Ackermann, "Algorithms for the calculation of scattering by stratified spheres," Appl. Opt. **20**, 3657–3660 (1981).

38. K. A. Fuller, W. C. Malm, and S. M. Kreidenweis, "Effects of mixing on extinction by carbonaceous particles," J. Geophys. Res. **104**, 15941–15954 (1999).

39. G. Lesins, P. Chylek, and U. Lohmann, "A study of internal and external mixing scenarios and its effect on aerosol optical properties and direct radiative forcing," J. Geophys. Res. **107(D10)**, 4094, doi:10.1029/2001JD000973 (2002).

40. S. Mogo, V. E. Cachorro, A. de Frutos, and A. Rodrigues, "Absorption ångström exponents of aerosols and light absorbing carbon (lac) obtained from *in situ* data in Covilhã, central Portugal," J. Environ. Monit. **14**, 3174–3181 (2012).

41. K. Adachi, S. H. Chung, H. Friedrich, and P. R. Buseck, "Fractal parameters of individual soot particles determined using electron tomography: Implications for optical properties," J. Geophys. Res. **112**, D14202, doi:10.1029/2006JD008296 (2007).

42. E. F. Mikhailov, S. S. Vlasenko, I. A. Podgorny, V. Ramanathan, and C. E. Corrigan, "Optical properties of soot-water drop agglomerates: An experimental study," J. Geophys. Res. **111**, D07209, doi:10.1029/2005JD006389 (2006).

1. Introduction

Understanding the interaction of light absorbing carbon (LAC) aerosols with radiation is essential for interpreting remote sensing observations as well as for modeling the direct climate forcing effect of aerosols. The complex morphology and chemically heterogeneous composition of this class of aerosols presents a major challenge to modeling approaches based on rigorous electromagnetic scattering theory. Freshly emitted LAC particles are fractal-like aggregates that are characterized by the number of primary monomers N_s, the monomer radius a, the fractal dimension D_f, and the structural prefactor k_0. The aggregate morphology is described by the scaling relation [1]

$$N_s = k_0 \left(\frac{R_g}{a} \right)^{D_f},$$ (1)

where the radius of gyration is defined by

$$R_g = \sqrt{\frac{1}{N_s} \sum_{i=1}^{N_s} r_i^2},$$ (2)

and r_i is the distance of the ith monomer from the aggregate's center of mass.

   Aging of LAC in the atmosphere results in changes of the morphological and optical properties (e.g. [2–6]). The initially lacy structure of the aggregates collapses (i.e., the fractal dimension increases) on a time scale that is much shorter than the average lifetime of LAC aerosols in the atmosphere (e.g. [7–10]). At the same time, LAC is partially oxidized and becomes increasingly hydrophillic. This process is accompanied by condensation of various materials onto the LAC aggregate, such as sulfate [11], organic matter, water, or sea salt [12]. These liquid-phase materials are characterized by weak optical absorption at visible wavelengths. For this reason, we will collectively refer to the coating materials as "weakly absorbing" materials. Note, however, that at IR wavelengths the imaginary part of the refractive index of the coating materials, such as sulfate, can become comparable to that of LAC. Field measurements confirm that the majority of aged LAC aggregates are encapsulated in a shell of liquid-phase material [13] that is weakly absorbing at visible wavelengths. For a more detailed discussion of the physical and chemical processes that influence the morphology of aged LAC aerosols, see, e.g., [14,15] and references therein.

   Electromagnetic scattering computations for such morphologically complex particles are extremely demanding. Computations for realistic model particles are usually limited to a few case studies. On the other hand, operational applications, such as the computation of look-up tables of aerosol optical properties for remote sensing retrieval algorithms or for broadband radiative

transfer computations in climate models, require computations for a large range of parameters. This necessitates the introduction of simplifying assumptions. One approach is to introduce simplifications to the physics of the electromagnetic scattering problem. However, scattering of electromagnetic radiation by fractal aggregates is a highly complex process involving coherent near-field interactions among the primary monomers; it has been demonstrated that attempts to by-pass proper solutions to Maxwell's equations can introduce large errors for LAC aggregates (e.g. [16]). (For a general discussion about approximate methods for solving Maxwell's equations, see [17]). Probably the safer approach is to introduce simplifications to the particle morphology, and to validate the simplified model geometries by comparison with morphologically realistic models or with measurements (e.g. [11, 15, 18–20]). This is the approach that will be followed in the present study.

Various simplified model geometries have been applied in the past. The simplest model treats LAC and weakly absorbing aerosols as externally mixed (i.e. separate) homogeneous spheres, thus ignoring both the complex structure and heterogeneous chemical composition of realistic LAC aerosols internally mixed with weakly absorbing material. The simplest internal mixture model describes these aerosols as internally mixed homogeneous spheres. The homogeneous mixture is characterized by an effective refractive index, which can be computed by simple volume-mixing rules or by effective medium theory (EMT) [21, 22]. A simple model for an encapsulated geometry is a core-shell model consisting of a spherical LAC core that is concentrically coated with a spherical shell of weakly absorbing material. In the past it has often been tacitly assumed that this model gives a better representation of the optical properties of aged LAC aerosols than the external mixture and homogeneous internal mixture models, because it is, putatively, morphologically more realistic (e.g. [23]). Recent comparisons with morphologically realistic encapsulated aggregate models showed, indeed, that the external mixture model substantially underestimates the absorption cross section C_{abs}, and that the homogeneous internal mixture model overestimates C_{abs} [15]. However, it was also found that the core-shell model significantly underestimates C_{abs}; the error introduced by the core-shell model can even exceed that of the internal homogeneous mixture model [15]. An improved model was proposed based on a core-shell-shell geometry, consisting of a weakly absorbing core, an inner LAC shell, and an outer weakly absorbing shell [15]. Although this model yields a better representation of the optical properties of encapsulated LAC aggregates than the core-shell or homogeneous internal mixture models, it also has one main shortcoming. The multi-layer sphere model requires significantly more computational resources than a homogeneous sphere or core-shell model, thus making it difficult to use this model for operational purposes.

The work reported in [15] was limited to a few selected wavelengths and to an investigation of integrated optical properties relevant for climate forcing simulations. The present study goes beyond that by (i) extending the investigation to the entire spectral range from the UV-C to the mid-IR; (ii) adding an investigation of remote-sensing relevant quantities, such as the backscattering cross section, the angular distribution of the scattered radiance and polarization, and the absorption Ångström exponent; and (iii) introducing a new model particle (the "core-gray shell" model) that achieves an excellent representation of most aerosol optical properties of encapsulated LAC aggregates, while being computationally much less expensive than the previously discussed core-shell-shell model. Section 2 provides an introduction to the morphological models and the numerical methods for solving Maxwell's equations. In Sect. 3 we present and discuss the results of this study, and concluding remarks are offered in Sect. 4.
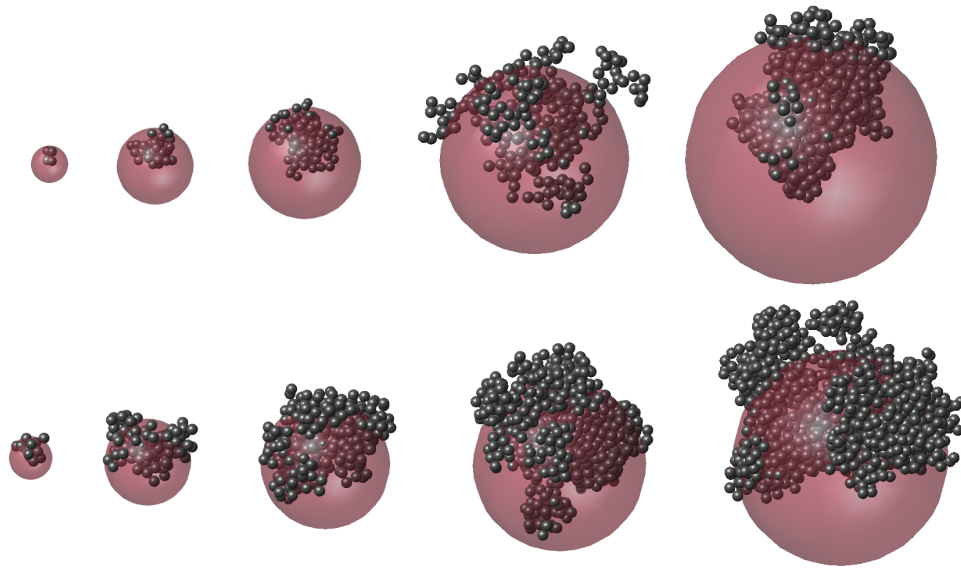
Fig. 1. Encapsulated aggregate geometries considered in this study. The particles have volume-equivalent radii of (from left to right) 100, 200, 300, 400, and 500 nm, and LAC volume fractions of 7 % (top row) and 20 % (bottom row).

2. Methods

2.1. Model particles

We solve Maxwell's equations for complex encapsulated aggregate morphologies of different sizes and volume fractions, as illustrated in Fig. 1. The parameters characterizing the morphological and dielectric properties of the encapsulated aggregates have been chosen based on field observations and laboratory studies such as to represent morphologically complex, aged LAC aerosols found in the atmosphere. More specifically, we fixed the fractal dimension and structural prefactor at D_f=2.6 and k_a=1.2, which are based on recent field observations of aged encapsulated LAC aggregates [13]. The radius of the primary LAC monomers of our model particles is 25 nm. Sensitivity studies have shown that this value gives the best agreement between modeled and measured single-scattering albedos of pure LAC aggregates [16], and it is consistent with recent field observations of aged encapsulated LAC aggregates [13]. The distance D_i between the centers of mass of the LAC aggregate and the weakly absorbing coating of radius R_{shell} has been chosen as D_i/R_{shell}=0.5, which is based on recent field observations [24]. Computations have been performed for a range of particle sizes between R_V=0.1–0.5 μm (where R_V denotes the volume-equivalent radius). As the total size R_V increases, both the number of monomers in the aggregate and the volume of the coating material increase accordingly, such that the volume fraction f remains constant (see Fig. 1 and Table 1).

   We limit our study to aggregates coated by a spherical shell. Electron micrographs of encapsulated aggregates with low LAC volume fractions often show that the coating is spherical or nearly spherical (e.g. [11, 12, 15, 25]). The reason for this is that the coating is in the liquid phase. Note, however, that for higher LAC volume fractions the coating may increasingly deviate from spherical shape; in the extreme case of LAC volume fractions approaching unity the coating will more or less assume the shape of a film covering the solid-phase LAC core. Such cases, which are more common for freshly emitted LAC near emission sources, are not

Table 1. Number of monomers N_s in the LAC aggregates and radius R_V of the internally mixed aerosols for LAC volume fractions $f=7\%$ and $f=20\%$. The radius R_V is the radius of a volume-equivalent sphere, where the volume of the encapsulated aggregates is the sum of the volumes of the LAC aggregate and the coating material. The monomer size is 25 nm for all values of N_s.

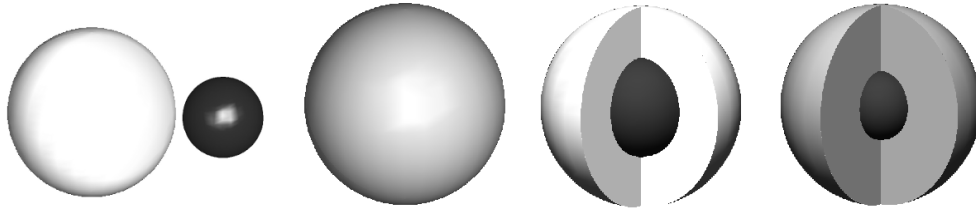|						
7 %	N_s	4	36	121	287	560
	R_V [nm]	96	200	300	400	500
20 %	N_s	13	102	346	819	1600
	R_V [nm]	101	200	300	400	500

Fig. 2. Simplified spherically symmetric model geometries (from left to right): External mixture, homogeneous internal mixture, core-shell, and core-gray shell.

considered in our study.

The study of the wavelength dependence of the optical properties focuses on the 14 wavelength bands used in numerical weather prediction model IFS (Integrated Forecasting System) developed at the European Centre for Medium Range Weather Forecast. The bands cover the range of 0.2–12.2 μm.

For each particle size we consider two LAC volume fractions, $f=7\%$ and $f=20\%$. The former is close to values reported in, e.g., [11,24]. However, as found in [24], volume fractions can display a high variability; far from emission sources LAC volume fractions are typically only a few percent. The higher value of $f=20\%$ is rather extreme. Such high volume fractions are mostly observed in aerosol plumes that have not traveled far from their emission sources (e.g. [13]).

The simplest model for representing encapsulated LAC aggregates is based on treating the weakly absorbing part and the LAC as externally mixed, i.e. separate, homogeneous spheres, as illustrated in Fig. 2 (left). Another simple model particle is the homogeneous internal mixture model (or "gray-sphere model", Fig. 2, second from left). Here we use the Maxwell Garnett mixing rule [26], which has been shown to work better than the commonly used volume-mixing rules [15], to compute the effective refractive index of the internal mixture. In the Maxwell Garnett rule, it is assumed that LAC inclusions are embedded in a matrix of weakly absorbing material, where the LAC inclusions are assumed to be small compared to the wavelength. A model that is, arguably, morphologically more realistic is the core-shell model (Fig. 2, second from right), in which the LAC is concentrated in a homogeneous sphere and concentrically coated by a shell of weakly absorbing material.

A known problem with all of these simplified model geometries is that they fail to mimic the amount of LAC mass that interacts with the electromagnetic field, which has a strong influence on the absorption cross section. Inside a solid LAC sphere the field is quickly attenuated, so that much of the mass near the core of the particle does not significantly contribute to the
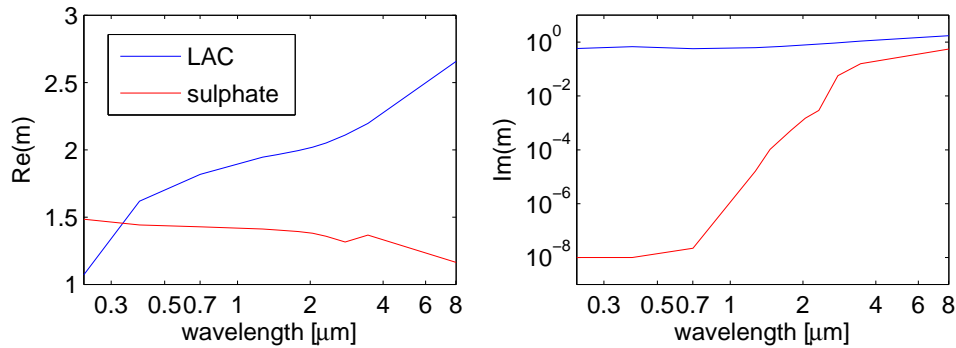
Fig. 3. Spectral variation of the real part (left) and imaginary part (right) of the refractive indices of LAC (blue) and sulfate (red).

absorption process. In an aggregate, a larger fraction of the LAC mass interacts with the field. For this reason, the external mixture and core-shell models tend to strongly underestimate the absorption cross section of encapsulated LAC aggregates. However, in an aged LAC aggregate of relatively high fractal dimension, at least some of the LAC mass is shielded from interacting with the external field. The homogeneous internal mixture model distributes the LAC mass too evenly and allows too high an LAC fraction to interact with the field, thus overestimating the absorption cross section. To overcome these limitations, a core-shell-shell model was recently proposed [15], consisting of a core of weakly absorbing material, an inner shell of LAC, and an outer shell of weakly absorbing material. Although this model was found to provide a good representation of the absorption cross section and single-scattering albedo of encapsulated aggregates, computations with this model are considerably more time consuming than computations with homogeneous sphere models or core-shell geometries. This severely limits the usefulness of this model for building an aerosol optics database that can be used in climate modeling or in inverse modeling of remote sensing observations.

Here we propose and test a different model that is computationally much faster than the core-shell-shell model, but also based on the notion that the most important aspect of a versatile model particle is the way in which the LAC mass is distributed within the weakly absorbing host, which determines the amount of LAC that is allowed to interact with the electromagnetic field. The model has a core-shell geometry. But by contrast to the original core-shell model (Fig. 2, second from right), the new model consists of a smaller core that only contains a fraction f_{core} of the LAC mass. The remaining fraction $(1 - f_{core})$ of the LAC mass is homogeneously mixed with the weakly absorbing shell, thus "darkening" the shell. This model is illustrated in Fig. 2 (right). For brevity, we shall refer to this geometry as the "core-gray shell" geometry. By reducing the size of the core, less LAC is shielded from interacting with the electromagnetic field. Most of the LAC mass that is homogeneously mixed with the weakly absorbing shell does interact with the field and contributes to absorption. The core fraction f_{core} is a free parameter that can be tuned to fit the reference calculations. This model appears to be sufficiently versatile to mimic the amount of LAC mass that interacts with the electromagnetic field in a realistic encapsulated aggregate, while maintaining a high degree of geometric simplicity and symmetry. Symmetry assumptions are the main factor in expediting numerical computations [27].

The dielectric properties assumed in this study are depicted in Fig. 3. By contrast to many other studies (e.g. [12]) we assume that the refractive index of LAC is dependent on wavelength. The spectral variation of the refractive index m of LAC in Fig. 3 is based on the measurements reported in [28]. In a recent review [29] it was found that many refractive indices of LAC

found in the literature are unrepresentative of LAC aerosols encountered in the atmosphere. The refractive index values observed in [28] are among the ones that lie closest to the recommendations given in [29] at a wavelength of 550 nm. However, we emphasize that we do not know if the measurements reported in [28] are equally realistic for atmospheric LAC aerosols at UV and IR wavelengths. The weakly absorbing material is assumed to be sulfate. Its spectral variation is based on values taken from the OPAC database [30]. As can be seen in the figure, $\text{Im}(m)$ of sulfate increases over several orders of magnitude in the near IR part of the spectrum.

2.2. Electromagnetic scattering computations

Electromagnetic scattering computations for the encapsulated aggregate model have been performed with the discrete dipole method, using the program DDSCAT described in [31], in conjunction with the Lattice-dispersion polarizability model [32].

Much efforts have been invested into testing the number of dipoles and the number of discrete Euler angles required in the numerical orientational averaging procedures. Among the tests conducted to ensure the correctness of results, we performed comparisons of DDSCAT computations for bare aggregates with numerically exact superposition T-matrix computations (using a program developed by Mackowski and Mishchenko [33]), as well as analyses of computed polarimetric differential scattering cross sections with the reciprocity condition [34]. For the latter tests, we employed the polarizability model described in [35]. We required that the reciprocity condition be fulfilled with an error of less than 3%. In order to reach such a high accuracy a dipole spacing d was required such that $|m|kd \leq 0.3$, where m denotes the complex refractive index of LAC, and k is the wavenumber in vacuum. Note that this dipole spacing is somewhat finer than the commonly recommended value of $|m|kd \leq 0.5$. The likely reason is that our encapsulated particle models contain a high degree of geometrical details, and we have a large dielectric contrast between LAC and sulfate. A more detailed account of how to test the accuracy of discrete dipole computations for bare and encapsulated aggregates is given in [15].

For homogeneous spheres we employed a Mie program described in [36]. Electromagnetic scattering computations for the core-shell geometries have been performed with the program developed by Wiscombe based on [37]. Effective refractive indices for homogeneous mixtures of LAC and sulfate were computed by use of the Maxwell Garnett mixing rule [26]. A comparison of this and other effective medium theories as well as volume-mixing rules applied to LAC mixed with weakly absorbing material can be found in, e.g., [15, 38, 39].

3. Results and discussion

3.1. Optical properties relevant for climate forcing of LAC

Figure 4 shows optical properties as a function of particle radius R_V and wavelength λ for aerosols with an LAC volume fraction of 7 % (where R_V is the volume-equivalent radius of the particle). More specifically, we present the absorption cross section C_{abs} (first row, left), the single-scattering albedo SSA (first row, center), and the asymmetry parameter g (first row, right) for the reference case, i.e. for encapsulated aggregates, as well as corresponding relative differences between these optical properties computed with different simplified model particles and those computed with the reference model (rows 2-5).

As expected, C_{abs} (top row, left panel) is monotonically increasing with R_V. The dependence on λ is less trivial; it reflects the dependence of C_{abs} on both the size parameter $x = 2\pi R_V/\lambda$ and the refractive indices of LAC and sulfate, which, in turn, also vary with wavelength. The external mixture model (second row, left) and, to a lesser extent, the core-shell model (fourth row, left) underestimates C_{abs}, while the homogeneous internal mixture model (third row, left) overestimates C_{abs}. This is most pronounced for large size parameters. The poor performance of these models is related to how the LAC mass is distributed throughout the particle. The external
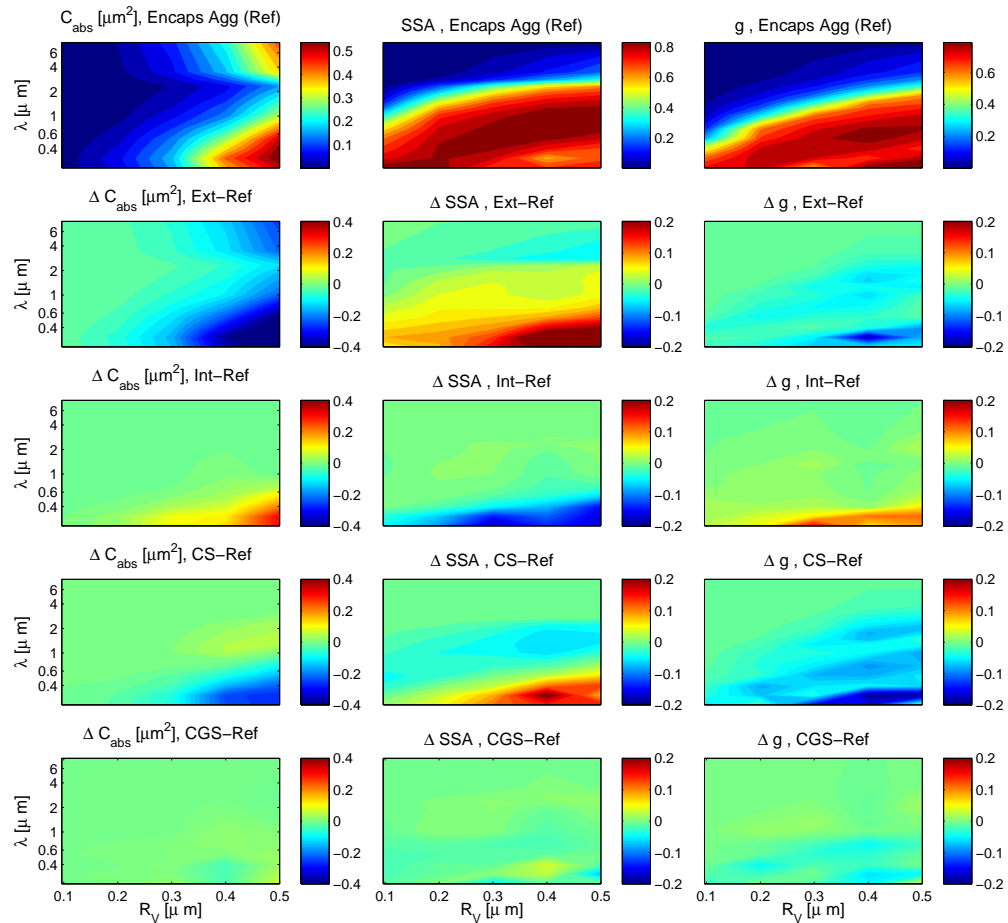
Fig. 4. C_{abs} (left), SSA (center), and g (right) as a function of particle size and wavelength for particles with an LAC volume fraction of $f=7$ %. The rows show reference results for encapsulated aggregates (first row), and relative differences between those and external mixtures (second row), internal homogeneous mixtures (third row), core-shell (fourth row), and core-gray shell particles (fifth row). Positive differences indicate that the simplified models overestimate the reference results.

mixture and core-shell models concentrate the LAC mass in a compact homogeneous sphere, in which too high a mass fraction is shielded from interacting with the electromagnetic field. The external mixture model suffers from an additional shortcoming. In a realistic encapsulated aggregate, the coating increases the geometrical cross section of the particle and focuses electromagnetic power onto the LAC aggregate, thus enhancing C_{abs}. While the core-shell model is capable of accounting for this effect, the external mixture model does not. The combined effect of neglecting focusing and concentrating the LAC mass in a compact sphere results in a strong underestimation of C_{abs} (second row, left). On the other hand, the homogeneous internal mixture model distributes the carbon mass too evenly throughout the sulfate host medium, which results in an overestimation of C_{abs} (third row, left).

These results help us understand the importance of simulating the optical properties of encapsulated LAC aerosols by using a model particle that attempts to mimic the distribution of LAC mass within the sulfate host particle. The model we propose here has, essentially, a core-shell geometry. However, we only concentrate a fraction f_{core} of the total LAC mass in the core, while the remaining fraction $(1 - f_{\mathrm{core}})$ is homogeneously mixed with the sulfate shell, using the Maxwell Garnett mixing rule for computing the effective refractive index of the shell. The fraction f_{core} residing in the core is a free parameter that can be adjusted to fit the reference computations.

Table 2. Choice of the core fraction f_{core} for each of the 14 wavelength bands (where λ denotes the band mid-point).

λ [μm]	0.2316	0.3040	0.3932	0.5332	0.7016	1.0101	1.2705
f_{core}	0.7	0.7	0.6	0.5	0.5	0.1	0.1
λ [μm]	1.4625	1.7840	2.0460	2.3250	2.7885	3.4615	8.0205
f_{core}	0.1	0.1	0.1	0.1	0.1	0.1	0.1

The bottom left panel in Fig. 4 shows the difference in C_{abs} computed with the core-gray shell model and the reference results obtained for the encapsulated aggregate model. A comparison of the left panels in rows 2–5 clearly shows the superior performance of the core-gray shell model in comparison to the other simplified model geometries.

The second column presents analogous results for the single scattering albedo SSA. This quantity displays a pronounced dependence on wavelength, and a somewhat weaker dependence on size (top center panel) than C_{abs}. Interestingly, the original core-shell model (fourth row, center) does not perform significantly better than the crude external mixture model (second row, center); both overestimate SSA at short wavelengths. By contrast, the homogeneous internal mixture model (third row, center) underestimates SSA at short wavelengths. By far the best results are achieved with the core-gray shell model. The maximum differences between that model and the reference results are almost an order of magnitude smaller than those introduced by the original core-shell model.

Similarly to SSA, the asymmetry parameter g (top right panel) displays a strong dependence on wavelength, and a weaker dependence on particle size. The homogeneous internal mixture model (third row, right) yields somewhat smaller maximum errors than the external mixture (second row, right) and the original core-shell model (fourth row, right). The largest errors are observed for short wavelengths. The core-gray shell model reproduces, again, the reference results most faithfully throughout the size and wavelength spectrum.

Table 2 shows the choices of f_{core} at different wavelengths that yielded the best agreement of the core-gray shell model with the reference computations. f_{core} is found to decrease with wavelength. These values are used throughout the paper for all particle sizes and for both LAC
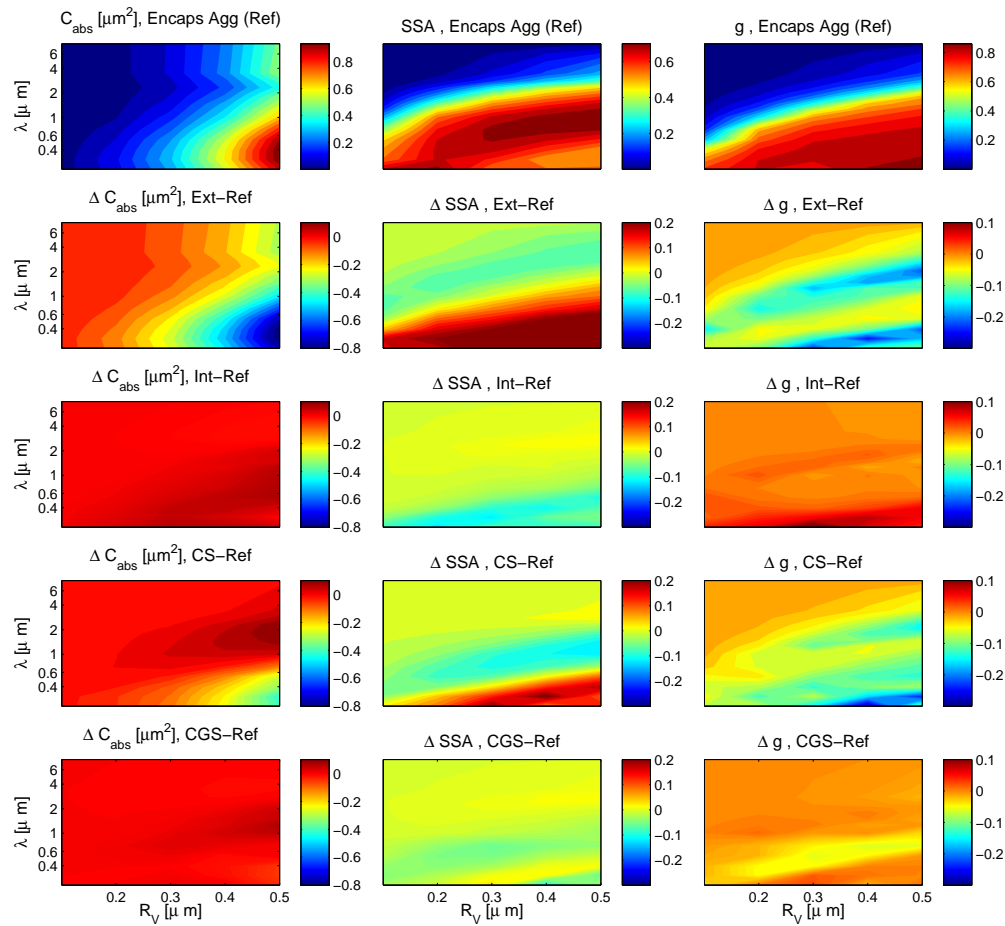
Fig. 5. As Fig. 4, but for f=20 %.

volume fractions, f=7 and 20 %. The fact that f_{core} is independent of f and R_V indicates that the optimal choices of the tuning parameter are rather robust.

Figure 5 shows results analogous to those in Fig. 4, but for aerosols containing an LAC volume fraction of 20 %. In general, the new core-gray shell model produces, again, quite satisfactory results. The problems with the original core-shell model become even more pronounced than for a volume fraction of 7 %. The homogeneous internal mixture model produces almost equally good results as the core-gray shell model for C_{abs} and SSA. However, for the asymmetry parameter g the homogeneous internal mixture model displays maximum errors that are somewhat larger than those of the core-gray shell. Note that the choices of f_{core} given in Table 2 were the same for both LAC volume fractions.

3.2. Optical properties relevant for remote sensing

The optical properties investigated thus far are those that are needed for modeling the radiative forcing effect of encapsulated LAC aerosols. We now turn to investigating optical properties relevant for remote sensing studies. Figure 6 shows the backscattering cross section C_{bak} as a function of size and wavelength for aerosols with an LAC volume fraction of 7 % (left column)
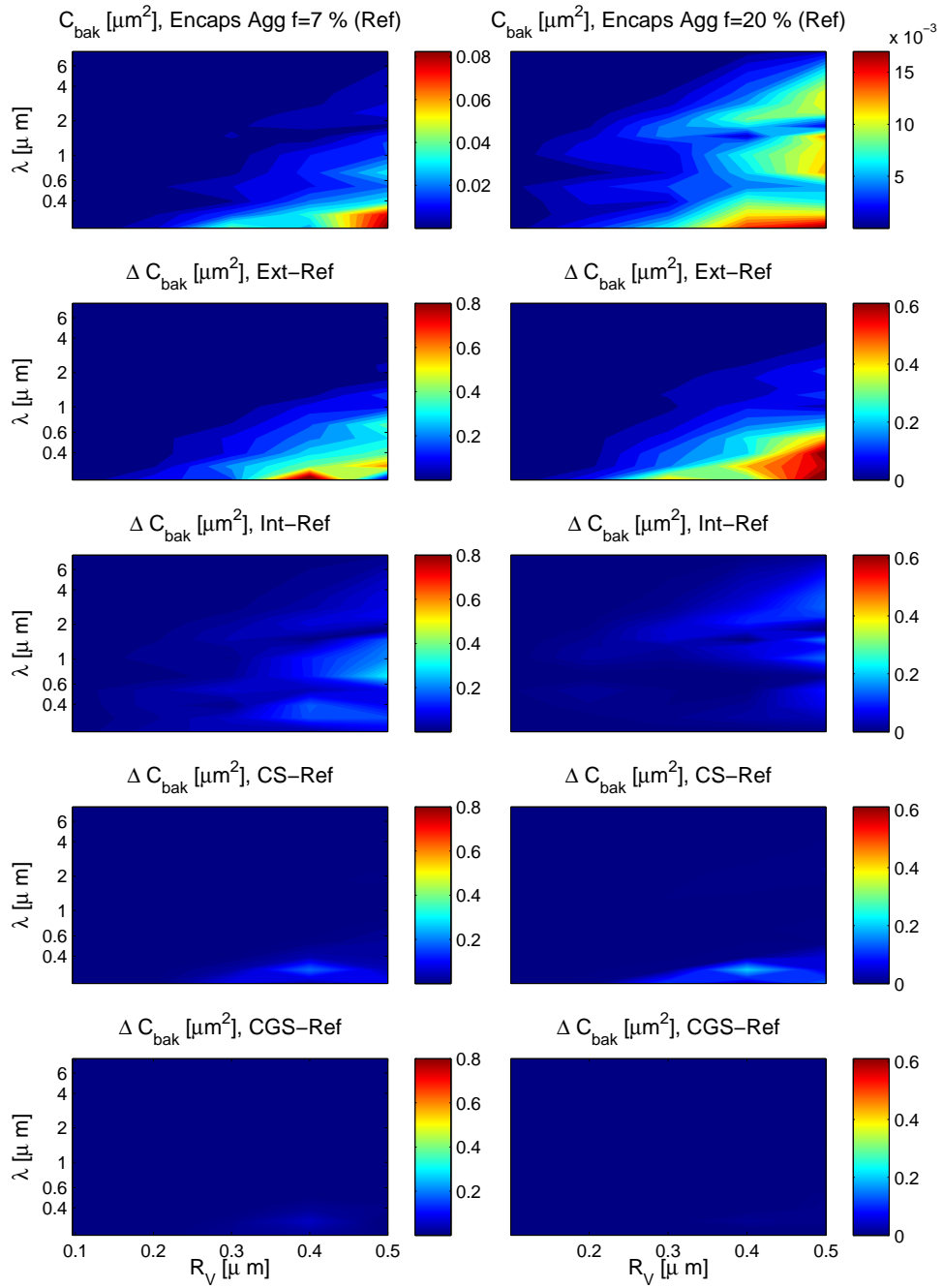
Fig. 6. Backscattering cross section for encapsulated aggregates with LAC volume fractions of f=7 % (top left) and f=20 % (top right), as well as differences between reference computations and results for simplified model particles.

and 20 % (right column). The top row shows the reference results obtained with the encapsulated aggregate model, while the other rows show differences between the reference results and those obtained with various simplified model geometries.

By comparing the two top figures, we can see that an increase in the LAC volume fraction from 7 % to 20 % decreases C_{bak} by roughly a factor of 5, which is quite dramatic. For f=7 %, C_{bak} changes by more than a factor of 4 as one increases the size parameter. Thus C_{bak} is about equally sensitive to changes in the LAC volume fraction as to changes in the size parameter.

Among the simple model particles, the external mixture model (second row) clearly performs worst; it produces results for C_{bak} that can be more than an order of magnitude larger than the reference results. This is likely to be caused by the high scattering cross section of the pure sulfate sphere in this model. The internal mixture model (third row) also yields very high errors, although not quite as high as the external mixture model. The original core-shell model (fourth row) and the core-gray shell model (fifth row) give reasonable results for a large range of sizes and wavelengths. The largest errors are observed in the UV, where the core-gray shell model yields significantly lower maximum errors than the original core-shell model. (A closer analysis reveals that these errors are caused by errors in the total scattering cross section, not by errors in the phase function in the backscattering direction.) The overall good representation of C_{bak} by the core-gray shell model is quite remarkable, because the free parameter f_{core} in that model has been optimized to yield a good fit of climate-relevant optical properties, not to reproduce C_{bak}.

In Fig. 7 we compare the Mueller matrix elements $\log F_{11}$ (left column), $-F_{12}/F_{11}$ (middle column), and F_{33}/F_{11} (right column) as a function of scattering angle and particle size at a wavelength of 304 nm. The LAC volume fraction is 7 %. Results are shown for encapsulated aggregates (first row), external mixtures (second row), homogeneous internal mixtures (third row), core-shell particles (forth row), and core-gray shell particles (fifth row). The Mueller matrix elements of the various simple model particles are quite similar to the reference results for encapsulated aggregates. Analogous observations hold for the Mueller matrix elements at other wavelengths and volume fractions (not shown). Thus the *relative* angular distribution of the scattered intensity is not highly sensitive to the employed particle model, nor is the angular dependence of the linear polarization. However, the *magnitude* of the scattered intensity will depend on the employed particle model, because the total scattering cross section does.

The reason why most Mueller matrix elements do not differ dramatically among the different particle models can be understood by inspecting Fig. 8. Here we show all six non-zero, independent Mueller matrix elements at a wavelength of 0.5332 μm. We compare computational results for encapsulated aggregates with an LAC volume fraction of 7 % and a total volume-equivalent radius R_V=0.5 μm (black), pure volume-equivalent sulfate spheres (red), and bare LAC aggregates (blue). The bare aggregates are exactly the same aggregates as those in the encapsulated geometry, except that they have been stripped of the coating. Apart from F_{22}, the Mueller matrix elements of pure sulfate spheres and encapsulated aggregates are very similar. This clearly shows that in the encapsulated aggregates the angular distribution of the scattered radiance and polarization is mostly determined by the sulfate coating (which is assumed to be spherical). The LAC aggregate inside the particle strongly influences, to be sure, the total scattering and absorption cross sections, thus the total scattered radiance, but not its *relative* angular distribution. Not surprisingly, the exception to this observation is the element F_{22}, which gives rise to depolarization. For spherically symmetric particles, $F_{11}=F_{22}$ holds identically for all scattering angles. The deviation of F_{22}/F_{11} from unity is a sensitive indicator of non-sphericity. Clearly, none of the simple model particles considered in this study is capable of reproducing the reference results, as all of these models are spherically symmetric particles. The non-sphericity of the LAC aggregate is responsible for the deviation of F_{22}/F_{11} from unity in the encapsu-
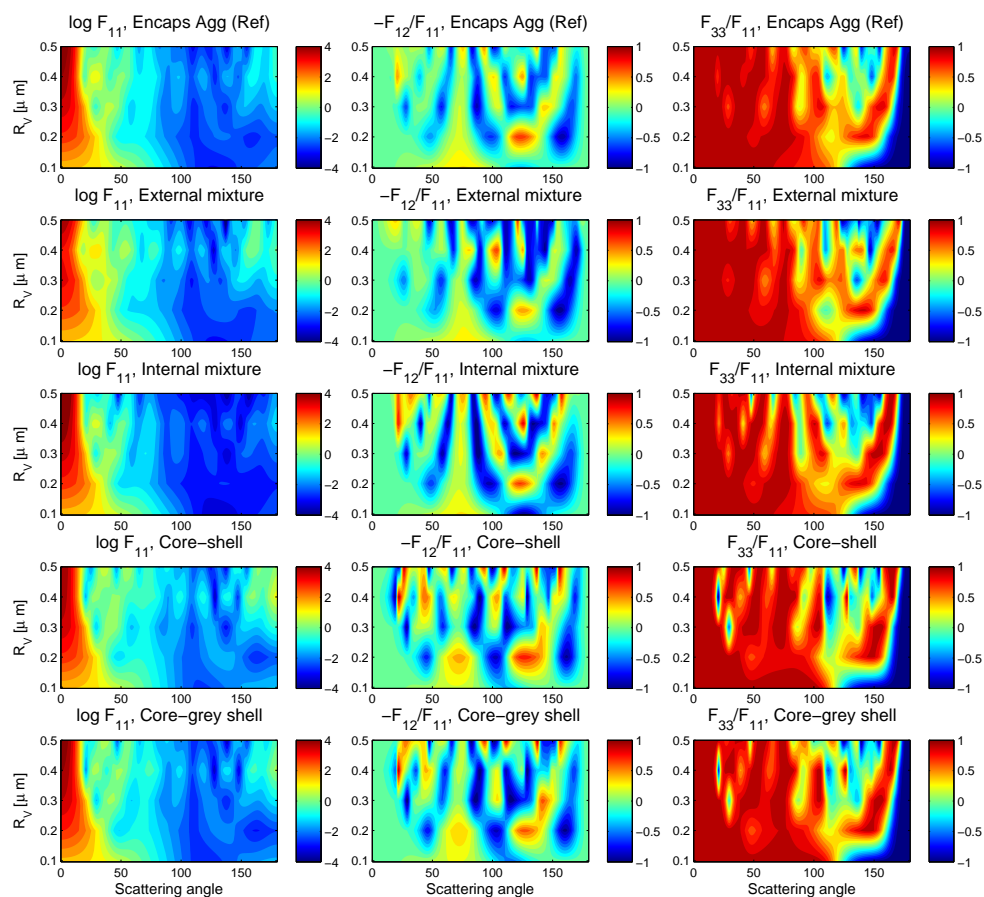
Fig. 7. Mueller matrix elements $\log F_{11}$ (left), $-F_{12}/F_{11}$, and F_{33}/F_{11} as functions of scattering angle and size at a wavelength of λ=304 nm. Results are shown for encapsulated aggregates (first row), external mixtures (second row), internal homogeneous mixtures (third row), core-shell (fourth row), and core-gray shell particles (fifth row).
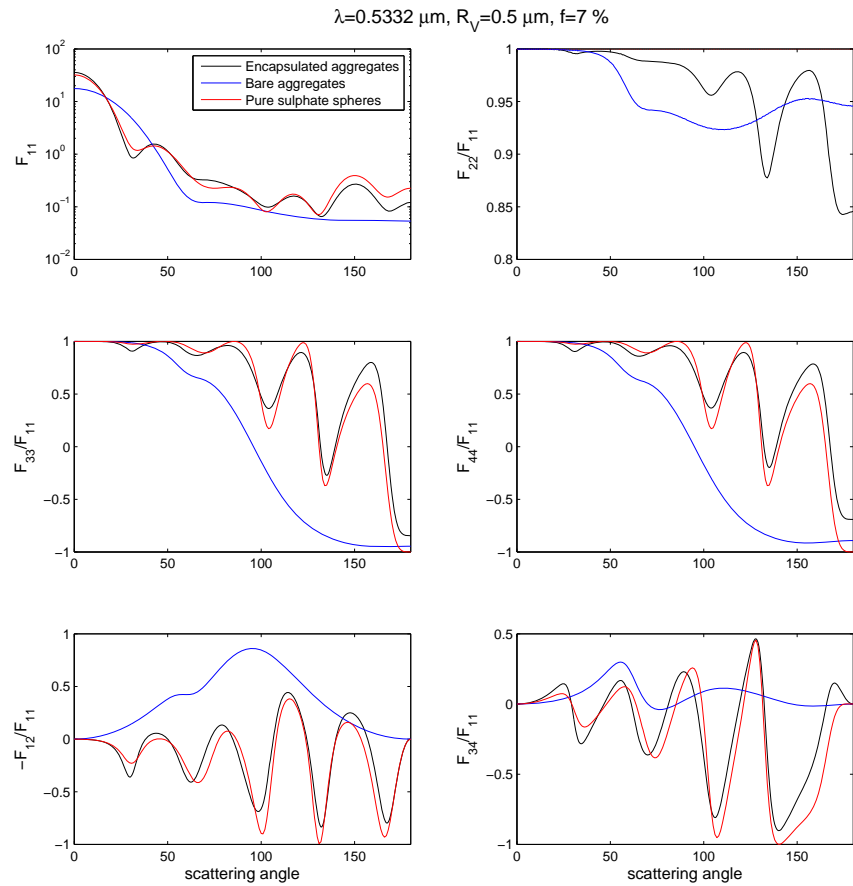
λ=0.5332 μm, R$_V$=0.5 μm, f=7 %

Fig. 8. Mueller matrix elements as a function of scattering angle for particles of a size R$_V$=0.5 μm at a wavelength of 0.5332 μm. Results are shown for encapsulated aggregates with an LAC volume fraction of 7 % (black), pure sulfate spheres (red), and bare aggregates (blue).

lated aggregates, but the spherical coating significantly alters F_{22}/F_{11} as compared to the pure aggregates.

One important implication is the following. If most of the Mueller matrix elements are determined by the sulfate coating, this means that the angular distribution of the scattered intensity and polarization is likely to be strongly sensitive to the shape of the coating. In this study we have limited our investigations to spherical coatings. However, the aggregate core can cause the coating to become distorted and deviate from spherical shape, especially for higher LAC volume fractions; this can strongly alter the Mueller matrix. Such effects are not investigated here.

Finally, we study the absorption Ångström exponent (AÅE), which we define for a wavelength interval $[\lambda_1, \lambda_2]$ according to

$$A\text{Å}E = -\frac{\ln \frac{C_{\text{abs}}(\lambda_1)}{C_{\text{abs}}(\lambda_2)}}{\ln \frac{\lambda_1}{\lambda_2}}. \tag{3}$$

For instance, AÅE=1 indicates that C_{abs} increases linearly with λ within a wavelength interval, while for AÅE=0 C_{abs} is independent of λ, and AÅE<0 in wavelength regions where C_{abs} decreases with λ. The limits of the wavelength intervals we considered are the values given in Table 2. For instance, the first interval at the short-wave end of the spectrum is given by λ_1=0.2316 μm, λ_1=0.3040 μm.

In Fig. 9 we plot this quantity as a function of size and of the mid-point wavelength $\lambda = (\lambda_1 + \lambda_2)/2$. The first row shows the reference results obtained for encapsulated aggregates with LAC volume fractions of f =7 % (left) and 20 % (right), and rows 2–5 show corresponding differences in the optical properties computed with the simplified model geometries and those obtained with the reference geometries.

We already saw in Figs. 4 and 5 that the wavelength dependence of C_{abs} does not follow a simple λ^{-1} dependence throughout the wavelength spectrum. As a consequence, AÅE changes significantly with wavelength. Comparison of the topmost panels in Fig. 9 with the top left panels in Figs. 4 and 5 shows that the spectral variation of C_{abs} is closely reflected by the wavelength dependence of AÅE.

The dependence of AÅE on particle size displays the characteristic monotonic decrease. Comparison of the top two panels also reveals that AÅE depends on the LAC volume fraction. An increase in the LAC volume fraction tends to enhance AÅE at wavelengths larger than 2 μm and reduce it at shorter wavelengths. In recent measurement campaigns AÅE values for wavelengths 470–660 nm were reported in the range from 0.86 to 1.47 [40]. These observations agree with our computational results for encapsulated aggregates with a low volume fraction of f=7 % (top row, left panel), which is more representative for aged LAC aerosols than the rather extreme case of f=20 %.

The internal mixture (third row) and core-gray shell models (fifth row) yield almost equally good representations of the reference results for high LAC volume fractions. However, for f =7 % the internal mixture model significantly overestimates AÅE for short wavelengths. The external mixture model (second row) and the original core-shell model (fourth row) mostly underestimate AÅE throughout the UV and visible part of the spectrum, especially for larger particle sizes. A use of these two models in size retrieval algorithms based on AÅE observations would therefore have a tendency to overestimate particle size. But note that for λ around 2.5 μm the original core-shell can strongly overestimate AÅE. The core-gray shell model (fifth row) represents AÅE reasonably well throughout the considered size and spectral ranges.

Let us try to understand why the external mixture and core-shell models yield lower AÅE values than the internal mixture and core-gray shell models, especially for particles of larger sizes. To this end, we first inspect the top left panels in Figs. 4 and 5, and we focus on the
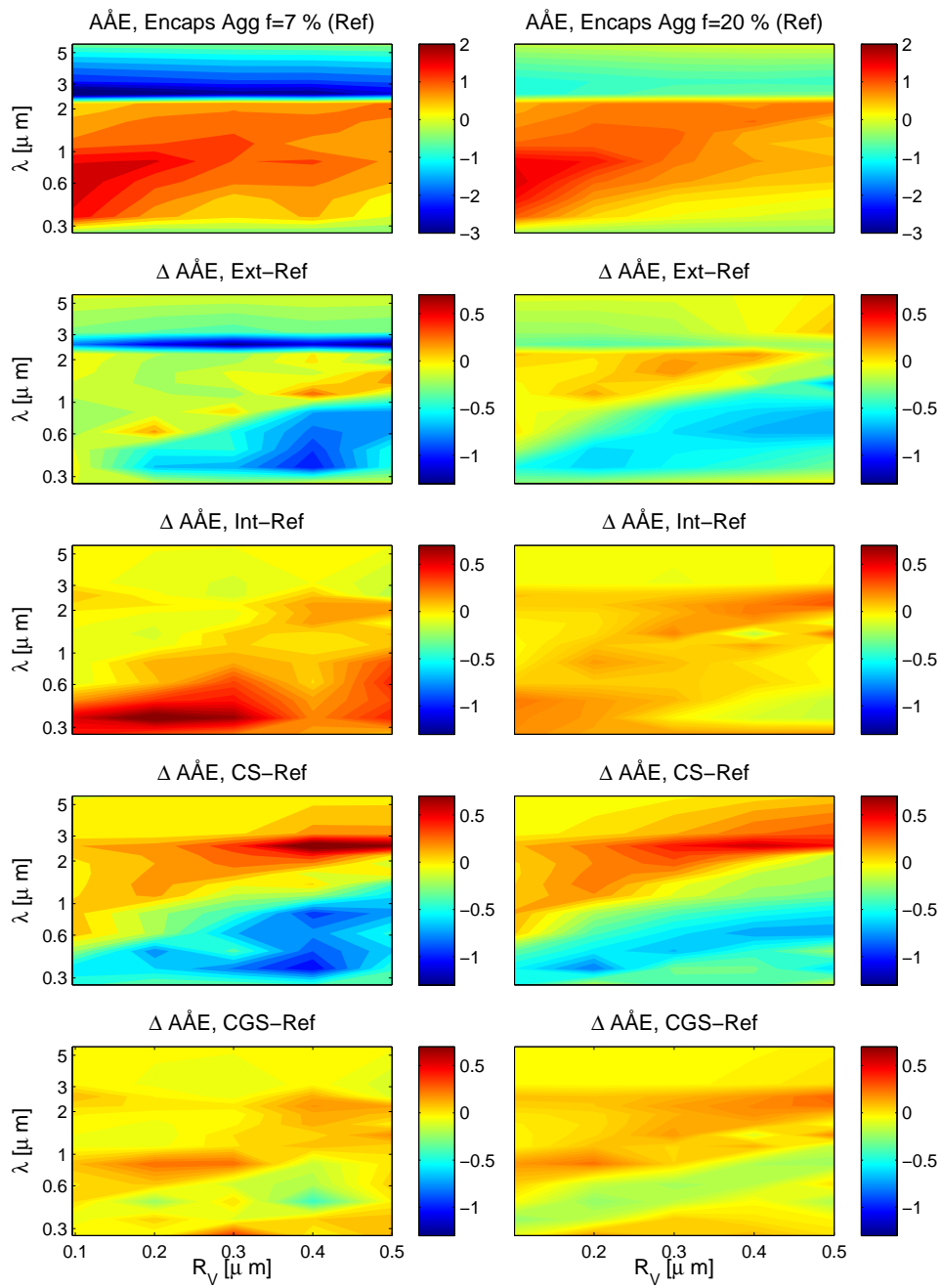
Fig. 9. As Fig. 6, but for the absorption Ångström exponent.

larger particle sizes. For both volume fractions, C_{abs} increases from the UV to the visible, followed by a decrease from the visible to the near IR. The external mixture (second row, left) and core-shell models (fourth row, left) display negative errors with a magnitude that increases slightly from the UV to the visible and then sharply decreases to the near IR. This means that the dependence of C_{abs} on wavelength is weaker for the external mixture and core-shell models than for the encapsulated aggregates, resulting in lower values of AÅE. This is much less pronounced for the internal mixture and core-gray shell models. What the external mixture and core-shell models have in common is that the sulfate is pure, while in the other two models it is homogeneously mixed with at least part of the LAC. In Fig. 3 (bottom) we see that the imaginary part of the refractive index $\text{Im}(m)$ of sulfate steeply increases from the visible to the near IR. An increase in wavelength reduces the size parameter of the particle, which results in a decrease in C_{abs}. However, the increase in $\text{Im}(m)$ partially compensates for this, thus flattening the decrease of C_{abs} with λ and reducing AÅE. By contrast, in the internal mixture and core-gray shell models the imaginary part of the effective refractive index of the sulfate-LAC mixture increases less rapidly with wavelength, because $\text{Im}(m)$ of LAC is almost constant with λ. As a consequence, for a given size, C_{abs} decreases more rapidly with wavelength from the visible to the mid-IR, resulting in higher values of AÅE.

4. Summary and conclusions

Modeling the optical properties of morphologically complex LAC aggregates encapsulated in a coating of weakly absorbing compounds is a highly challenging and computationally demanding task. Radiative forcing simulations in climate models as well as look-up tables for remote sensing retrieval algorithms require computations for a large range of aerosol parameters. Such comprehensive computations cannot be performed for realistic encapsulated aggregate models; one needs to rely on simplified model geometries. The present study aims at developing and testing such a model. It it an extension of previous efforts described in [15], in which only a limited set of wavelengths and only climate-relevant optical properties have been considered. In the present study, we considered the entire spectral range from the UV-C to the mid-IR, and we investigated both climate- and remote sensing-relevant optical properties. The model introduced in [15] was quite accurate, but it proved to be too slow for use in more extensive calculations, as required for generating look-up tables of aerosol optical properties. By contrast, the model introduced in the present study is highly accurate and computationally inexpensive. The main findings are:

- The most critical factor in designing a simple model particle is to mimic the amount of LAC mass that can interact with the electromagnetic field. This is determined by how the LAC mass is distributed within the weakly absorbing host material. Most commonly employed simple model particles fail to take this important factor into account.

- For example, contrary to common believes (e.g. [23]), a simple core-shell geometry does not produce reliable estimates of the optical properties of encapsulated LAC aggregates. In many cases, this model falls short of the even cruder homogeneous internal mixture model.

- Our proposed "core-gray shell" model is found to realistically mimic the amount of LAC that interacts with the electromagnetic field. In this model only part of the LAC resides in the core, while the remaining part is homogeneously mixed with the weakly absorbing material in the concentric coating. For a suitable choice of the fraction f_{core} of LAC residing inside the core, this model is found to give the best overall agreement with the absorption cross section, single-scattering albedo, and asymmetry parameter computed

for the encapsulated LAC aggregates. These optical properties are important for accurate estimates of the radiative forcing effect of LAC.

- Although f_{core} in the core-gray shell model has been optimized for reproducing climate-relevant optical properties, we found that the core-gray shell model also gives the best representation of optical properties relevant for remote sensing applications. In reproducing the backscattering cross section and absorption Ångström exponent, it outperforms the conventional core-shell model as well as the external mixture and homogeneous internal mixture models. The elements of the Mueller matrix (except F_{22}) are rather insensitive to the choice of model particle, as they are largely determined by the spherical coating. The F_{22} element, being a sensitive indicator of particle nonsphericity, cannot be reproduced by any simplified model particle with perfect spherical symmetry.

- The optimal choices of f_{core} are independent of particle size and LAC volume fraction, which indicates that the tuning of the core-gray shell model is rather robust. However, f_{core} does depend on wavelength.

The improvements achieved with the core-gray shell model are particularly pronounced for low LAC volume fractions, which are most representative for aged, internally mixed LAC aerosols in the atmosphere.

Table 3. Fractional bias *FB* and, in parentheses, normalized root mean square error *NRMSE* for the four different model particles and for different optical properties.

	external mixture	internal mixture	core-shell	core-gray shell
C_{abs}	-0.66 (0.08)	0.06 (0.14)	0.01 (0.21)	0.01 (0.05)
SSA	0.00 (0.24)	-0.02 (0.07)	0.01 (0.10)	0.00 (0.03)
g	-0.16 (0.12)	0.03 (0.05)	-0.14 (0.08)	-0.01 (0.04)
C_{bak}	12 (17)	8.8 (3.9)	0.93 (2.5)	0.00 (0.33)
AÅE	-0.14 (2.2)	0.11 (1.0)	0.09 (3.7)	-0.02 (0.39)

Table 3 shows the fractional bias *FB* and the normalized root mean square error *NRMSE* for the different models and for different optical properties. These quantities are defined in terms of the reference results x_i^{ref} and the results x_i^{mod} obtained for different model particles as

$$FB = \frac{\sum_i (x_i^{\text{mod}} - x_i^{\text{ref}})}{\frac{1}{2}\sum_i (x_i^{\text{mod}} + x_i^{\text{ref}})} \tag{4}$$

$$NRMSE = \sqrt{\frac{\sum_i (x_i^{\text{mod}} - x_i^{\text{ref}})^2}{\sum_i (x_i^{\text{ref}})^2}}, \tag{5}$$

where x denotes any of the optical properties, and where the index i runs over all sizes, wavelengths, and LAC volume fractions considered in this study. This is a highly aggregated presentation of the detailed results shown in the preceding sections that leaves out a lot of the information about the dependence of model errors on size, wavelength, and volume fraction. However, this summary does provide a concise overview of the overall performance of different models for different optical properties. For instance, the external mixture model consistently underestimates C_{abs} (note the large magnitude of *FB* combined with the low value of *NRMSE*). Thus, when performing climate forcing calculations involving averaging over sizes, wavelengths, and LAC volume fractions, this model is guaranteed to underestimate the radiative forcing effect

of LAC. On the other hand, the core shell model has a rather low fractional bias for C_{abs}, but a very high value of *NRMSE*. It is therefore quite unpredictable to what extent averaging over sizes, wavelength, and LAC volume fractions will partially cancel the large positive and negative errors that this model will inevitably introduce. The most important observation is that the new core-gray shell model introduced here consistently yields the lowest fractional biases and normalized root mean square errors.

We emphasize, once more, that there are potentially important factors that this study did not account for. First, only a limited number of reference geometries has been used. We did consider aggregates of different sizes and volume fractions, but we did not investigate the variation of the optical properties with fractal parameters, monomer size, or position of the aggregate within the host material. Field measurements indicate that these parameters vary among different samples (e.g. [13, 41]). Also, the host material was assumed to be sulfate, while LAC aggregates in nature can be coated with a mixture of different compounds, such as sulfate, organic substances, sea salt, and water. Coatings of different chemical compositions will have different effective refractive indices. Thus we do not claim that our particular choices for the free parameter f_{core} given in Table 2 work equally well under all conditions. Another important limitation of this study is that the coating of the LAC aggregates was assumed to be spherical. The presence of nonspherical coatings will strongly impact the angular distribution of the scattered intensity and polarization.

In summary, the main practical consequence of this investigation is that we have introduced the core-gray shell particle as a fast and flexible model that can realistically mimic the amount of LAC mass that contributes to absorption and scattering in coated LAC aggregates. This model, with suitable choices of the free parameter f_{core}, was found to accurately represent integrated and differential scattering optical properties of morphologically complex encapsulated aggregates. However, our choices for the free parameter in the core-gray shell model may only be valid for the specific reference geometries considered in this study. Therefore, the general recommendation is to further explore the usefulness of the core-gray shell model in more extensive case studies; this should involve modelling studies that consider different coating materials, LAC geometries, and volume fractions, as well as comparison with atmospheric measurements or laboratory experiments (e.g. [42]).